

Research Article: New Research | Sensory and Motor Systems

## Chronometry on Spike-LFP Responses Reveals the Functional Neural Circuitry of Early Auditory Cortex Underlying Sound Processing and Discrimination

Arpan Banerjee<sup>1,2</sup>, Yukiko Kikuchi<sup>2,3,4,5</sup>, Mortimer Mishkin<sup>4</sup>, Josef P. Rauschecker<sup>5</sup> and Barry Horwitz<sup>2</sup>

<sup>1</sup>Cognitive Brain Dynamics Lab, National Brain Research Centre, NH-8, Manesar, Gurgaon, Haryana 122052, India

<sup>2</sup>Brain Imaging and Modeling Section, National Institute on Deafness and Other Communication Disorders, National Institutes of Health, Bethesda Maryland, USA

<sup>3</sup>Institute of Neuroscience, Newcastle University Medical School, Newcastle upon Tyne, UK

<sup>4</sup>Laboratory of Neuropsychology, National Institute of Mental Health, Bethesda Maryland, USA

<sup>5</sup>Department of Neuroscience, Georgetown University Medical Center, Washington, DC, USA

DOI: 10.1523/ENEURO.0420-17.2018

Received: 5 December 2017

Revised: 24 May 2018

Accepted: 25 May 2018

Published: 6 June 2018

**Author Contributions:** AB, YK, MM, JPR, BH designed research; AB, YK & BH performed research; AB and YK analyzed data; AB, YK, MM, JPR and BH wrote the paper.

**Funding:** <http://doi.org/10.13039/501100001407>Department of Biotechnology, Ministry of Science and Technology (DBT) BT/RLF/Re-entry/31/2011 BT/07/IYBA/2013

**Funding:** <http://doi.org/10.13039/100000065HHS> | NIH | National Institute of Neurological Disorders and Stroke (NINDS) R01 NS052494

**Funding:** <http://doi.org/10.13039/100000089NSF> | Office of International Science and Engineering (OISE) PIRE OISE 0730255

**Conflict of Interest:** Authors report no conflict of interest.

This work was supported by grants from the Department of Biotechnology, Govt. of India (Grant Nos BT/RLF/Re-entry/31/2011 and BT/07/IYBA/2013) to A.B., from NIH/NINDS (R01 NS052494) and NSF (PIRE OISE-0730255) to J.P.R., and by the Intramural Research Programs of NIMH (M.M., Y.K.) and NIDCD (A.B., B.H., Y.K.).

**Correspondence should be addressed to:** Arpan Banerjee, [arpan.nbrc@gov.in](mailto:arpan.nbrc@gov.in) or [banerjee2007@gmail.com](mailto:banerjee2007@gmail.com)

**Cite as:** eNeuro 2018; 10.1523/ENEURO.0420-17.2018

**Alerts:** Sign up at [eneuro.org/alerts](http://eneuro.org/alerts) to receive customized email alerts when the fully formatted version of this article is published.

Accepted manuscripts are peer-reviewed but have not been through the copyediting, formatting, or proofreading process.

Copyright © 2018 Banerjee et al.

This is an open-access article distributed under the terms of the Creative Commons Attribution 4.0 International license, which permits unrestricted use, distribution and reproduction in any medium provided that the original work is properly attributed.

1

2 **1.Title: Chronometry on spike-LFP responses reveals the functional neural**  
3 **circuity of early auditory cortex underlying sound processing and**  
4 **discrimination**

5 **2.Abbreviated Title:** Chronometry in macaque auditory cortex

6 **3. Authors:**

7 Arpan Banerjee<sup>1,2,\*</sup>, Yukiko Kikuchi<sup>2,3,4,5</sup>, Mortimer Mishkin<sup>4</sup>, Josef P. Rauschecker<sup>5</sup>, Barry  
8 Horwitz<sup>2</sup>

9 **Affiliations**

- 10 1. Cognitive Brain Dynamics Lab, National Brain Research Centre, NH-8, Manesar, Gurgaon -  
11 122052, Haryana, India  
12 2. Brain Imaging and Modeling Section, National Institute on Deafness and Other  
13 Communication Disorders, National Institutes of Health, Bethesda, Maryland, USA  
14 3. Institute of Neuroscience, Newcastle University Medical School, Newcastle upon Tyne, UK  
15 4. Laboratory of Neuropsychology, National Institute of Mental Health, Bethesda, Maryland,  
16 USA  
17 5. Department of Neuroscience, Georgetown University Medical Center, Washington, D.C.,  
18 USA

19

20 **4. Author Contributions:** AB, YK, MM, JPR, BH designed research; AB, YK & BH  
21 performed research; AB and YK analyzed data; AB, YK, MM, JPR and BH wrote the paper  
22

23 5. Correspondence should be addressed to (include email address): [arpan.nbrc@gov.in](mailto:arpan.nbrc@gov.in),  
24 [banerjee2007@gmail.com](mailto:banerjee2007@gmail.com)

**6. Number of Figures** 6

**7. Number of Tables** 1

**8. Number of  
Multimedia** NA

**9. Number of words for Abstract** 237

**10. Number of words for Significance  
Statement** 119

**11. Number of words for Introduction** 748

**12. Number of words for Discussion** 2019

25 **13. Acknowledgements**

26 This work was supported by grants from the Department of Biotechnology, Govt. of India  
27 (Grant Nos BT/RLF/Re-entry/31/2011 and BT/07/IYBA/2013) to A.B, from NIH/NINDS (R01  
28 NS052494) and NSF (PIRE OISE-0730255) to J.P.R., and by the Intramural Research Programs  
29 of NIMH (M.M., Y.K.) and NIDCD (A.B., B.H., Y.K.). A.B. acknowledges Prof. Neeraj Jain  
30 (National Brain Research Centre, India) for helpful comments. We wish to thank Dr. Brian  
31 Scott for useful comments and for a detailed reading of an earlier version of this paper.

#### 32 **14. Conflict of Interest**

33 Authors report no conflict of interest

#### 34 **15. Funding sources**

35 1. Department of Biotechnology, Govt. of India (Grant Nos BT/RLF/Re-entry/31/2011 and  
36 BT/07/IYBA/2013) to AB

37 2. NIH/NINDS (R01 NS052494) to JPR

38 3. NSF (PIRE OISE-0730255) JPR

39 4. Intramural Research Programs of NBRC, India

40 5. Intramural Research Programs of NIMH and NIDCD.

41

42

43 **Title: Chronometry on spike-LFP responses reveals the functional neural circuitry of**  
44 **early auditory cortex underlying sound processing and discrimination**

45

46 **Abstract**

47 Animals and humans rapidly detect specific features of sounds, but the time courses of the  
48 underlying neural response for different stimulus categories is largely unknown. Furthermore,  
49 the intricate functional organization of auditory information processing pathways is poorly  
50 understood. Here, we computed neuronal response latencies from simultaneously recorded spike  
51 trains and local field potentials (LFPs) along the first two stages of cortical sound processing,  
52 primary auditory cortex (A1) and lateral belt (LB), of awake, behaving macaques. Two types of  
53 response latencies were measured for spike trains as well as LFPs: 1) *Onset latency*, time-locked  
54 to onset of external auditory stimuli, and 2) *selection latency*, time taken from stimulus onset to  
55 a selective response to a specific stimulus category. Trial-by-trial LFP onset latencies  
56 predominantly reflecting synaptic input arrival typically preceded spike onset latencies,  
57 assumed to be representative of neuronal output indicating that both areas may receive input  
58 environmental signals and relay the information to the next stage. In A1, simple sounds, such as  
59 pure tones, yielded shorter spike onset latencies compared to complex sounds, such as monkey  
60 vocalizations ('coos'). This trend was reversed in LB, indicating a hierarchical functional  
61 organization of auditory cortex in the macaque. LFP selection latencies in A1 were always  
62 shorter than those in LB for both PT and Coo reflecting the serial arrival of stimulus-specific  
63 information in these areas. Thus, chronometry on spike-LFP signals revealed some of the  
64 effective neural circuitry underlying complex sound discrimination.

65

66 **Significance statement**

67 Auditory core (A1) and lateral belt (LB) areas are key subdivisions of auditory cortex. A1 plays  
68 crucial role in processing of simple stimuli such as pure tones whereas LB for processing of  
69 complex sounds. Both areas receive direct inputs from medial geniculate nucleus and have  
70 recurrent connections. Nonetheless, the functional connectivity patterns between these  
71 subdivisions while processing different sound categories are poorly understood. Using  
72 simultaneous spike-LFP recordings our study reveals that information about the presence of a  
73 stimuli in the environment arrive concurrently in core and LB, however the information related  
74 to neuronal discrimination may arrive at different times indicating both parallel and serial  
75 information transmission pathways exist and their presence is guided by the context of the task.  
76

77 **Introduction**

78 Simple auditory stimuli such as pure tones are represented as tonotopic maps in primary  
79 auditory cortex (Hind, 1953, Merzenich et al., 1976, Romani et al., 1982, Morel et al., 1993)  
80 whereas belt areas, lateral and medial to the core, while still showing cochleotopic organization,  
81 process more complex features of sounds (Muscari et al., 1990, Rauschecker et al., 1995, Tian  
82 and Rauschecker, 2004, Recanzone, 2008, Kuśmierk and Rauschecker, 2009, Niwa et al.,  
83 2013, Kikuchi et al., 2014). The core is primarily defined based on the thalamic connections  
84 from the ventral division of the medial geniculate nucleus (MGN) and reciprocally connected  
85 with the adjacent subdivisions of the belt (Hackett, 2011, Scott et al., 2015). Thus, the  
86 functional organization of complex sounds in core and belt can be hypothesized to follow a  
87 serial processing stream, from core to belt, somewhat analogous to V1 and the V2/V4/MT areas  
88 of the visual system (Tian et al., 2013). At the same time, direct inputs from the medial  
89 geniculate nucleus to these brain areas point to parallel processing pathways (Rauschecker et al.,  
90 1997), which continue further downstream (Sheline et al., 2010). Finally, demands of a task,  
91 such as sound localization, categorization, and discrimination, can also govern the serial versus  
92 parallel characterization of processing (Ahveninen et al., 2006, Ahveninen et al., 2013, Bizley  
93 and Cohen, 2013).

94  
95 Chronometry of input and output related processing events in candidate brain areas is a useful  
96 technique for functional network identification (Kreiman et al., 2006, Nielsen et al., 2006,  
97 Monosov et al., 2008, Banerjee et al., 2010, 2012). While neuronal spike discharge is used as a  
98 measure of output processing in a putative brain area (Kruger and Becker, 1991, Middlebrooks  
99 et al., 1994, Nawrot et al., 2003, Buzsaki et al., 2012), local field potentials (LFPs) may carry  
100 information about the inputs coupled with local neuronal processing that need not be input-

101 specific, in a particular brain area (Gusnard et al., 2001, Nielsen et al., 2006, Buzsaki et al.,  
102 2012) and by extending this principle to multiple brain areas, aspects of the functional circuitry  
103 underlying behavior can be revealed (Hung et al., 2005, Banerjee et al., 2012) (Figure 1).  
104 Conceptually, shorter latencies in one area compared to another reflect faster processing and  
105 greater relevance of the former brain area and thus indicate more efficient neuronal coding  
106 (Gawne et al., 1996, Van Rullen and Thorpe, 2001, Bendor and Wang, 2008). Additionally, the  
107 timing of input versus output of information processing in an area can be used to infer the role  
108 of this area in processing of a particular type of signal as well as the functional pathways  
109 involved in processing of the signal (DiCarlo and Maunsell, 2005).

110

111 Spike trains and LFPs in auditory core exhibit comparable frequency tuning (Kayser et al.,  
112 2007). On the other hand, there is evidence suggesting that the cochleotopic organization of belt  
113 areas is less precise, as observed in spike-LFP responses (Guo et al., 2012). Hence, identifying  
114 the temporal markers of inputs and outputs involved in information processing in auditory core  
115 and belt across single units and populations can help reveal the functional specificity of the  
116 respective areas. Extending this line of reasoning, Camalier and colleagues computed neuronal  
117 onset latencies at different locations along the auditory cortical pathways and reported that  
118 dorsal stream locations have shorter latencies, whereas the ventral locations exhibit  
119 increasingly longer latencies as one proceeds from lower to higher-order processing (Camalier  
120 et al., 2012). This result conforms with human studies using magnetoencephalography and  
121 transcranial magnetic stimulation (Ahveninen et al., 2006, Ahveninen et al., 2013) as well as  
122 with other monkey studies (Scott et al., 2011, Kuśmierk and Rauschecker, 2014). Kikuchi et  
123 al. (2014) reported that pure tone (PT) related spike onset latencies were longer in lateral belt

124 (LB) than in auditory core, which is consistent with the notion that auditory core is at a lower  
125 hierarchical level within cortex than LB. However, do the two areas receive information about  
126 stimulus presence concurrently? Furthermore, are the finer features that allow discrimination of  
127 one signal from another represented in the neural codes hierarchically?

128 To address these questions, we recorded spike and LFP responses simultaneously from A1 and  
129 LB of two adult macaques while they performed an auditory Go/No-go discrimination task. We  
130 computed trial-by-trial *Onset Latency*, time locked to stimulus onset, and *Selection Latency*, the  
131 earliest time at which neural responses between PTs and Coos significantly differ. Computing  
132 these measures in different sub-divisions of auditory cortex we could tease out the functional  
133 network mechanisms involved in sound processing and discrimination.

134 **Methods**

135 ***Animal preparations and behavioral task***

136 Two adult male Rhesus macaques (*Macaca mulatta*, weighing 7.5-11.5 kg) participated in this  
137 study. Animal care and all procedures were conducted in accordance with the National Institutes  
138 of Health guidelines and were approved by the Georgetown University Animal Care and Use  
139 Committee. Animals were prepared for chronic awake electrophysiological recordings under  
140 aseptic conditions. Each animal was anesthetized and a head post and recording chamber were  
141 attached to the dorsal surface of the skull with a guidance of MRI obtained with a 3T scanner  
142 (0.5 mm voxel size, Siemens Tim Trio). The recording sites in this study cover the auditory core  
143 (primary auditory cortex, A1) and the auditory LB region (the middle lateral [ML] and  
144 anterolateral [AL]). We followed identical methods for assigning the recording sites to either  
145 A1 or LB as described in Kikuchi et al. (2014).

146 Electrophysiological experiments were conducted in a single-walled acoustic chamber  
147 (Industrial Acoustics Company, Bronx, NY) installed with foam isolation elements (AAP3,  
148 Acoustical Solutions). The animal sat in a monkey chair with its head fixed, facing a speaker  
149 located one meter directly in front of it in a darkened room. The animal was trained to perform  
150 an auditory discrimination task, in which a single positive stimulus (S+), consisting of a 300-ms  
151 pink-noise burst (PNB), was pseudo-randomly interspersed among negative stimuli (S-),  
152 consisting of all other stimuli, for 20% of the trials. The animal initiated a trial by holding a  
153 lever for 500 ms, triggering the presentation of one of the acoustic stimuli, was required to  
154 release the lever within a 500-ms response window after the offset of the S+ to get a water  
155 reward (~0.2 ml) that followed by a 500-ms inter-trial interval (ITI). Lever release in response  
156 to S- prolonged the 500-ms-ITI by one second (timeout). The average inter-stimulus-interval

157 was  $2.3 \pm 0.45$  s (mean  $\pm$  SD). The detailed procedures for the animal preparations, behavioral  
158 task, and data collection were the same as those described in Kikuchi et al. (2014).

159

160 ***Sound preparation and stimuli***

161 The sound waveform signals were sent from the CORTEX dual-computer system through a 12-  
162 bit D/A converter (CIO-DAS1602/12, ComputerBoards), and then amplified, attenuated, and  
163 delivered through a free-field loudspeaker (Reveal 6, Tannoy) with a flat ( $\pm 3$  dB) frequency  
164 response from 63 Hz to 51 kHz.

165

166 The monkey vocalizations ('Coo' calls) were recorded in Morgan Island using a directional  
167 microphone (ME66 with K6 powering module, Sennheiser, CT, USA, frequency response at 40-  
168 20,000 Hz  $\pm$  2.5 dB) with a solid-state portable recorder (PMD670, Marantz Professional,  
169 London, UK) at a sampling rate of 48 kHz (Laboratory of Neuropsychology, NIMH). Pure tones  
170 (PTs) and PNBs were created using Adobe Audition 1.5 at a sampling rate of 48 kHz (32 bit).  
171 All stimuli had a 300-ms fixed duration, including the monkey vocalizations, gated with a 5-ms  
172 rise/fall linear ramp. The stimuli were normalized across all stimuli by recording the stimuli  
173 played through the stimulus presentation system, and filtering the recorded signal on the basis of  
174 Japanese macaque audiograms (Jackson et al., 1999), and using the maximum root-mean-square  
175 (RMS) amplitude during a sliding window of 200 ms duration and presented at  $\sim 70$ dB SPL.  
176 Details of the sound equalization method were described by Kuśmierk and Rauschecker  
177 (2009).

178 The positive stimulus was a pink noise, a response to which led to a reward, whereas the  
179 negative stimuli were made up of both pure tones (PTs) and "coo" vocalizations. A stimulus set

180 comprised of 10 PTs and 10 pitch-matched Coo, in which the fundamental frequency (F0) of the  
181 Coo was match to the corresponding frequency of PT using the pitch-shift function in Adobe  
182 Audition 1.5 (Figure 2). The frequency of PTs and the F0 of the coos ranged from G3 (196 Hz)  
183 to C#8 (4435 Hz) in 6 semitone steps. In each recording session, the stimuli were presented in  
184 pseudorandom order with at least 15 trials per stimulus.

185

186

187 ***Data collection and pre-processing***

188 Multiple guide tubes carrying up to 4 tungsten microelectrodes (0.5-3.0 M $\Omega$ , epoxytite  
189 insulation, FHC, Bowdoin, ME) was lowered into the target cortical sites identified on the MRI  
190 scans. Each electrode was independently advanced using a remote-controlled hydraulic, four-  
191 channel customized multidrive system (NAN-SYS-4, Plexon. Inc., Dallas, TX). For the spike  
192 trains, raw signals were filtered with a band-pass of 150-8000 Hz, further amplified, and then  
193 digitized at 40 kHz. For the LFP, the raw voltage traces were filtered between 0.7 and 500 Hz,  
194 amplified, and digitized at 1 kHz. For further analyses, the LFP data were low-pass filtered at  
195 100 Hz. Time stamps for stimulus presentation timings, behavioral response, and reward  
196 delivery were sent through DOS-CORTEX dual computer system (CIO-DAS1602/12, CIO-  
197 DIO24, ComputerBoards). Spikes were sorted by real-time acquisition programs using template  
198 matching and Principal Component Analysis (PCA) methods (RASPUTIN, Plexon). We  
199 focused on trials in which simultaneous spike-LFP recordings were obtained from both  
200 monkeys in both core and LB areas. Overall, we accumulated data from 29 sessions in Monkey1  
201 and 27 sessions from Monkey2, for a total of 56 sessions, where a session was defined as a  
202 group of trials for which we obtained simultaneous spike train recordings from one neuron in  
203 A1 and one in LB. Two sessions may have different single cells (spike-sorted) but the same LFP

204 representation. We aggregated all 23 fundamental frequencies presented to the monkeys under a  
205 single category called “pure-tone (PT)” trials. Similarly, all F0-matched monkey calls were  
206 categorized as “Coos”. This enhanced the statistical power of our analytical framework but did  
207 not adversely affect the main goals of the study. Hence, to increase the statistical power of our  
208 analysis, we chose to categorize all pure-tone trials as one block and the F0-matched Coo trials  
209 as a different block. Firing rates reported in Figure 3 were computed from binary spike rasters  
210 by applying Gaussian smoothing with a 10-ms window on the averaged peri-stimulus histogram  
211 (PSTH) with a bin size of 1 ms. The mean evoked LFP waveform was calculated by averaging  
212 LFPs across trials.

213

214

### 215 *Trial-averaged latency analysis*

216 Histograms of binary spiking events were computed using 1-ms bins and were convolved with  
217 growth-decay functions (Thompson et al., 1996, Monosov et al., 2008) to compute continuous  
218 spike density functions (SDF). Time constants for growth phase,  $\tau_g = 1\text{ ms}$  and for decay  
219 phase,  $\tau_d = 20\text{ ms}$  were used to compute the spike density functions following Thompson et al  
220 (1996). A ms-by-ms t-test was applied to the two SDFs either within different temporal  
221 segments of the same trial (for onset) or between trials from different conditions (for  
222 discrimination) to obtain the onset and selection latencies, respectively, over an entire session  
223 (Figure 4). As LFPs are continuous signals, the raw LFP traces (band-passed between 0-200 Hz)  
224 were used to compute onset and selection latencies. Pairwise Wilcoxon rank-sum tests were  
225 performed to establish significant effects. We report the statistical analysis performed on data  
226 pooled from both monkeys and set a threshold of  $p = 0.01$  for estimating significance. We set

227 the threshold to this slightly conservative value since there were a large number of trials in each  
228 session that were available for the trial-by-trial analysis (below).

229

### 230 ***Trial-by-trial AccLLR analysis***

231 Spike trains and local field potentials (LFP) follow different statistical properties and hence the  
232 estimation of single-trial latencies from these two signals requires a unified framework  
233 (Banerjee et al., 2010, 2012). AccLLR addresses this issue and computes spike-LFP latencies  
234 trial-by-trial (Figure 5). AccLLR is a model-based framework that requires two competing  
235 models of observations. We have used time-varying firing rate models for spiking  
236 (inhomogeneous Poisson process) and time-varying continuous means and standard deviations  
237 (Gaussian process) for LFP signals. For further discussion on different kinds of models, see  
238 Banerjee et al. (2010, 2012). Once the model parameters (time-dependent firing rate for spikes  
239 and mean and standard deviation for LFP) are computed from a set of training trials, the  
240 likelihood that the time series for a test trial (binary spike trains for spikes, continuous  
241 waveform for LFP) belongs to model 1 or model 2 can be computed. Finally, raw spike trains  
242 and continuous LFPs can be transformed into the space of accumulated log-likelihood ratios by  
243 first calculating likelihood ratios (LR)

$$244 \quad LR(t) = \frac{P(x(t)| Model 1)}{P(x(t)| Model 2)} \quad 1$$

245 where  $x(t)$  is the data point at which LR is computed. To compute the  $LRs$  we use the leave-  
246 one-out principle. The trial at which LR was computed, doesn't contribute to obtaining the  
247 model parameters. The rest of the trials are used in model development. This was done to  
248 minimize the bias of any particular model.

249 By integrating the natural logarithm of  $LR(t)$  over time we obtain accumulated log-  
250 likelihood ratios ( $AccLLR(t)$ ), which follow a drift-diffusion process (Gold and Shadlen, 2001,  
251 Eckhoff et al., 2008, Banerjee et al., 2010). Thus, the difference in statistical properties of spike  
252 trains and LFPs become inconsequential in the space of AccLLRs, which unifies these  
253 measurements. Latencies are computed setting bounds specific to a model (1 or 2) of AccLLRs  
254 (see Figure 6).

255 An important aspect of the AccLLR framework is that it sets the bounds on the  
256 accumulation of integrated log-likelihood ratios, ordinarily done using the sequential probability  
257 ratio test (SPRT) (Wald and Wolfowitz, 1947). Under this framework, accumulated log-  
258 likelihood ratios obtained using equation 1 reaches a decision threshold after “sufficient”  
259 information has been collected. Alternatively, information is sufficient to make a decision when  
260 a certain threshold is reached. At an asymptotic limit, a mathematical relationship connecting  
261 the location of bounds of AccLLR accumulation to false positive and false negative rates can be  
262 expressed (Wald and Wolfowitz, 1947).

263 For the purpose of decoding latencies within a biologically relevant time, we chose a data-  
264 driven approach to set the bounds on AccLLR accumulation (Banerjee et al., 2010). For a given  
265 post-stimulus event as model 1, there are two possibilities for detection within a finite time, viz,  
266 whether the event is correctly detected (true positive) or no detection is possible (false  
267 negative). On the other hand, for the pre-stimulus baseline (null) as model 2, either correct (true  
268 negatives) or incorrect (false positives) assignment is made. For setting a bound for onset  
269 detection, we chose an optimum threshold for which the false positive rate for null data equals  
270 or exceeds the detection of the true positive rate on event data. For setting bounds for selection  
271 latency detection, we first computed the AccLLRs for a “null” period (pre-stimulus baseline),

272 300 ms from the start of a trial. There are three potential outcomes; AccLLR reaches i) an  
273 upper threshold corresponding to hit rate for model 1, ii) a lower threshold corresponding to hit  
274 rate for model 2, and iii) doesn't reach either threshold ("don't know"). Again, the threshold for  
275 detecting model 1 was chosen at an optimal point where the probability of "don't knows"  
276 exceeds the hit rate for model 1. Similarly, the threshold for detecting model 2 was chosen at an  
277 optimal point where the probability of "don't knows" exceeds the hit rate for model 2 (Figure  
278 6). For further details, see Banerjee et. al (2012).

279 While decoding latencies at the level of single trial brings us close to revealing the true nature  
280 of neural processing occurring at a realistic time scale, nonetheless, the process of choosing a  
281 threshold is impacted by speed-accuracy trade off, meaning a lower threshold can make  
282 detection faster while increasing the false positives, and on the other hand a higher threshold  
283 can increase accuracy but also increase the onset and selection latencies. Hence to check that  
284 the consistency of latency results are extended to situations where accuracy is set at 100%, we  
285 pooled all log-likelihood ratios from all trials within a session to create a pseudo-trial.  
286 Accumulated log-likelihood ratios were computed on this trial for each detection context, onset  
287 and selection. AccLLR threshold for onset detection was chosen to be the maximum AccLLR  
288 reached by a "null" trial. Similarly, AccLLR threshold for selection of one category of stimulus  
289 (model 1) was determined by the maximum reached by AccLLR from the second category  
290 (model 2).

291

292 **Results**

293 Spike-LFP recordings were obtained simultaneously from two brain areas, A1 in the auditory  
294 core and lateral belt (LB). Our recordings in LB came from two subdivisions, anterolateral (AL)  
295 and middle lateral (ML) belt areas. Here, we were interested in trials where simultaneous spike-  
296 LFP recordings were obtained from both monkeys in both A1 and the LB areas. We  
297 accumulated 29 sessions in Monkey1 and 27 sessions in Monkey2, totaling 56 sessions in which  
298 simultaneous spike-LFP recordings were obtained in A1 and LB. We computed the *onset*  
299 *latency* of the neural response of either spike or LFP using the method of accumulated log-  
300 likelihood ratios (AccLLR, for details see Banerjee et al. 2010). According to this framework,  
301 for single/multi-unit spiking activity, the baseline can be the background firing rate during the  
302 pre-stimulus period. Analogously, in the case of LFP, the baseline can be the distribution of  
303 voltage traces during the pre-stimulus period. We computed the timing of information  
304 processing events from trial-by-trial spike-LFP data (for further details of the method see  
305 Banerjee et al. 2010, 2012).

306 Monkeys performed the auditory discrimination task in a Go/No-go setup illustrated in  
307 Figure 2. Monkeys were trained to discriminate different kinds of sounds (all negative, or No-go  
308 cues) from a pink noise stimulus (positive, or Go cue), which, when responded to, resulted in a  
309 water reward. Onset latency and selection latencies were computed from spike-LFP responses.  
310 Onset latency characterized the boundaries of a processing stage required for encoding the  
311 presence of sound in the environment, thereby a measure of *stimulus-related processing*. On the  
312 other hand, selection latency characterized the boundaries of a processing stage involved in  
313 coding the presence of a specific sound in the environment, hence yielding a measure of  
314 *stimulus-specific* processing. Figure 3 illustrates an example recording session in each monkey.

315 In Monkey1, we observed a transient increase in spike frequency around the beginning and end  
316 of the stimulus in A1, whereas we saw sustained spiking responses in LB. Simultaneously, a  
317 difference in LFP waveforms is observed during stimulus presentation for the two stimulus  
318 categories. In Monkey2, we observed sustained firing in A1 following a transient rise of spike  
319 rate at stimulus onset. Furthermore, LFP differences were observed primarily between two  
320 stimulus categories in a period following the termination of stimulus presentation. These  
321 examples illustrate the diversity and complexity of spike/LFP responses across different  
322 recording sessions in both A1 and LB.

323

#### 324 **Chronometry on spike-LFP responses**

325 We computed neuronal response latencies for onset and discrimination using two approaches: a  
326 traditional trial-averaged approach and single-trial AccLLR analysis (Banerjee et al., 2010) of  
327 spike-LFP data. The former gives a broad summary of the results, and the latter helps in  
328 addressing the between-trial variability in neural signals and gives a more consistent account of  
329 neuronal information processing. In the first approach, a ms-by-ms t-test (Monosov et al, 2008)  
330 was used to compute **trial-averaged** measures of latencies. This approach is a standard one,  
331 used by most investigators. In the second approach, the AccLLR framework was used to  
332 compute **trial-by-trial** latencies of onset and selection (Banerjee et al., 2012). Additionally we  
333 applied ms-by-ms t-test on trial-by-trial AccLLR distributions for each session to compute the  
334 trial averaged latencies. In both cases, simultaneously collected data from two brain regions  
335 (A1 and LB) were used. We report statistics performed over all sessions from two monkeys in  
336 both the text (p-values) and Table 1 (mean and standard error of the mean (SEM)).

337

338 ***Trial-averaged latencies from raw data***

339 *Ms-by-ms t-test* was applied to raw LFP traces and spike distribution functions (see Methods for  
340 details) to extract spike-LFP latencies as followed by an earlier study (Monosov et al 2008).  
341 Analyses of the combined data from both monkeys are presented in Figure 4a and in Table 1  
342 (results from each monkey are also presented separately in Figure 4) for a sample size of 56  
343 sessions (29 for Monkey 1 and 27 for Monkey 2). Note that we rounded latencies to whole  
344 numbers for reporting group averages and that  $p = 0.01$  was chosen as the threshold in pairwise  
345 t-tests used to evaluate the statistical significance of both trial-averaged and AccLLR analysis  
346 across stimuli categories and brain areas. For pure tones, mean LFP onset latency in A1 (45 ms)  
347 was not significantly different ( $p = 0.22$ ) from mean LFP onset latency in LB (57 ms). The  
348 same was true not true for Coo ( $p = 0.001$ , mean 29 ms in A1, 45 ms in LB). However, the  
349 stimulus-specific differences between LFP onset latencies (i.e., between PT and Coo) were  
350 significant in A1 ( $p < 0.01$ ) but not in LB ( $p = 0.02$ ).

351 Mean spike onset latencies for PT were 87 ms in A1 and 103 ms in LB. Mean spike  
352 onset latencies for Coo were 63 ms in A1 and 83 ms in LB. No stimulus-specific differences  
353 were observed for spike onset latencies (PT vs. Coo) in either A1 ( $p = 0.1$ ) or LB ( $p = 0.25$ ).  
354 However, spike-LFP onset latency differences in A1 and LB were significant for both stimuli  
355 (PT and Coo;  $p < 0.01$  for all four comparisons). These results suggest that inputs arrive at A1  
356 and LB from a shared source and that there is considerable parallel processing across the two  
357 areas.

358 Trial-averaged selection latencies are computed from ensembles of trials belonging to  
359 two stimulus categories. That is, one selection latency value is defined for two stimulus  
360 categories for each session of recording. LFP selection latencies in A1 and LB were not

361 significantly different ( $p = 0.44$ , mean 111 ms in A1 and 121 ms in LB; detailed statistics are  
362 presented in Table 1). Similarly, spike selection latencies across A1 and LB were also not  
363 significantly different ( $p = 0.41$ , mean 140 ms in A1 and 164 ms in LB).

364 Spike-LFP selection latency differences were not significant in LB ( $p < 0.01$ ) and Core  
365 ( $p = 0.03$ ) with the threshold level set at  $p = 0.01$ . Thus, hierarchical stimulus processing from  
366 A1 to LB cannot be inferred from this analysis. A largely similar pattern of results was observed  
367 when the analysis was repeated for each monkey separately (Figure 4a).

368

#### 369 *Trial-averaged latencies from AccLLR estimates*

370 AccLLR at the level of single trials is a probabilistic method dependent on accumulation  
371 evidences. Inherently, it has a “slowness” incorporated to it which is further dependent on signal  
372 to noise ratios. Hence to get a sense of the speed-accuracy trade-off that affects AccLLR  
373 analysis we applied *ms-by-ms t-tests* on distribution of AccLLRs to compute the trial-averaged  
374 latencies (Fig 4b and in Table 1). This will give an estimate of latencies that can be achieved  
375 with maximum accuracy using AccLLR analysis for the ensemble of trials and sessions.

376 Mean LFP onset latency for pure tone was 60ms in A1 and 57ms in LB and was not  
377 significantly different ( $p = 0.61$ ). Mean LFP onset latency for Coo was 51 ms in A1 and 55 ms  
378 in LB and was not significantly different ( $p = 0.09$ ). The stimulus-specific differences between  
379 LFP onset latencies (i.e., between PT and Coo) were not significant in A1 ( $p = 0.06$ ) and LB ( $p$   
380  $= 0.02$ ).

381 Mean spike onset latencies for PT was 67 msec in A1 and 87 ms in LB which were not  
382 statistically significant ( $p = 0.73$ ). Mean spike onset latencies for Coo were 74 ms in A1 and 94  
383 ms in LB which were not significantly different ( $p = 0.62$ ). We didn't find any stimulus-specific

384 differences for spike onset latencies (PT vs. Coo) in A1 ( $p=0.45$ ) and LB ( $p=0.47$ ). Spike-LFP  
385 latencies were significant different for Coo in A1 ( $p=0.01$ ) but not for PT ( $p=0.58$ ). ). Spike-  
386 LFP latencies were not significantly different in LB for both Coo ( $p=0.03$ ) and PT ( $p=0.02$ )  
387 stimuli.

388 LFP selection latencies in A1 (155 ms) and LB (170 ms) were not significantly different ( $p=$   
389 0.25). Analogously, spike selection latencies in A1 (89 ms) and LB (106 ms) were not  
390 significantly different ( $p=0.24$ ). No significant differences were found between spike –LFP  
391 selection latencies in A1 ( $p=0.06$ ) and LB ( $p=0.25$ ).

392

### 393 *Trial-by-trial AccLLR analysis*

394 AccLLR (Banerjee et al., 2010) was used to compute trial-by-trial onset and selection latencies  
395 (Figure 5 and Table 1). Spike and LFP data were transformed to AccLLR space using  
396 inhomogeneous Poisson models for spikes and Gaussian models for LFP. Latencies were  
397 computed by setting decision bounds on AccLLR time series. For onset latency estimation,  
398 model 1 was applied to spike/LFP data during the stimulation period and model 2 to pre-  
399 stimulus baseline; for selection latency, model 1 was applied to PT trials and model 2 to Coo  
400 trials (see Methods for details). Latencies were estimated using the leave-one-out rule, where  
401 model parameters were estimated from all other trials leaving aside the one for which the  
402 latency was being computed. Two major advantages of using the AccLLR method were that we  
403 could reduce the variability observed in the trial-averaged analysis and that the stimulus-specific  
404 selection latencies could be computed trial-by-trial. On the other hand, a definition of single  
405 selection latency encompasses at least two trial categories for trial-averaged analysis. The  
406 AccLLR analysis had orders of magnitude higher sample sizes than those in the trial-averaged

407 analysis (Table 1). Theoretically, unlike the raw data, AccLLRs from both spike and LFP  
408 follow the same statistical distribution (see Methods for details), hence spike-LFP comparisons  
409 are quantitatively valid. The mean and SEM for onset and selection latencies are reported in  
410 Table 1.

411 The mean LFP onset latencies in A1 and LB for PT stimuli were nearly identical (35 ms in  
412 A1, 36 ms in LB,  $p = 0.10$ ). On the other hand, the mean LFP onset latency for Coos differed  
413 significantly in the two areas (31 ms in A1, 39 ms in LB,  $p < 0.01$ ). Spike onset latencies  
414 differed significantly between A1 and LB for PTs (52 ms in A1, 92 ms in LB,  $p < 0.01$ ). For  
415 Coos, the difference in spike onset latencies between A1 and LB is small but significant (69 ms  
416 in A1, 66 ms in LB,  $p < 0.01$ ). Together, these results suggest that processing relatively simpler  
417 stimuli like PT can be supported by A1, whereas more complex stimuli such as Coos require  
418 resources of a higher order area such as LB. LFP onset latencies always preceded spike onset  
419 latencies in each area and each stimulus category ( $p < 0.0001$ ).

420 Interestingly, for either type of stimulus, LFP selection latencies were always shorter in A1  
421 than in LB (for PT, means of 113 ms in A1 vs. 161 ms in LB,  $p < 0.01$ ; for Coos, 111 ms in A1,  
422 167 ms in LB,  $p < 0.01$ ), whereas spike selection latencies were always shorter in LB than in  
423 A1. For PT, spike selection latency was 187 ms in A1 and 163 ms in LB,  $p < 0.01$ ; and for Coos,  
424 178 ms in A1 vs. 155 ms in LB,  $p < 0.01$ . Most interestingly, for Coos the LFP selection latency  
425 (167 ms) lagged the spike selection latency (155 ms) significantly ( $p < 0.01$ ).

426

427 ***Estimates from pooled trials with 100% accuracy***

428 To evaluate if the pattern of results holds in a scenario where detection accuracy is 100%  
429 (thus taking into consideration the effects of speed-accuracy trade-off), we pooled all trials in a

430 session to create a single trial in the log-likelihood space . Details of procedures of how  
431 thresholds were selected are described in the Methods section.

432 The LFP mean onset latencies for PT was very similar in A1 and LB (see Table 1), a  
433 difference of 8ms which was not significant ( $p = 0.03$ ). A similar pattern followed for Coo ( $p =$   
434  $0.26$ ). A1 seems to have lower LFP onset latency for PT (26 ms) compared to Coo (38 ms) but  
435 the effect was weak ( $p = 0.01$ ). In LB the LFP mean onset latencies were identical for PT (30  
436 ms) and Coo (31 ms) ( $p = 0.87$ ). A similar pattern followed for mean spike onset latencies, and  
437 as well was observed for LFP. When spike-LFP latencies were compared except in A1 for PT  
438 where spike-LFP latencies were not different ( $p = 0.12$ ), LFP latencies typically precede spike  
439 latencies.

440 Mean selection latencies for LFP were much lower than that obtained with single trial  
441 measures however the main pattern of LFP selection latencies being lower in A1 compared to  
442 LB was consistent ( $p < 0.0001$ ). The mean spike onset latencies were in close proximity and none  
443 of the comparisons was significant at  $p = 0.01$ . Even the spike-LFP latency differences were not  
444 significant for individual selection contexts, for PT in A1 ( $p = 0.33$ ), Coo in A1 ( $p = 0.1$ ), PT in  
445 LB (0.60), and Coo in LB ( $p = 0.93$ ).

446

447 ***Decoding performance***

448 An important requirement in any decoding analysis framework is to control for the false  
449 positives and false negatives while setting thresholds for category distinction. In principle, the  
450 AccLLR test is optimal (Wald and Wolfowitz, 1947). Under conditions in which sufficient  
451 information is available or after infinite accumulation, the number of times any threshold is  
452 crossed is circumscribed by type 1 and type 2 errors. However, we are interested in latencies  
453 which would be biophysically relevant and computed using comparable statistical constraints on  
454 spike trains and LFP data. Detection of latencies within a finite time is constrained by a trade-  
455 off between accuracy and early detection (Figure 6a). Hence, we have chosen a data-driven  
456 approach to set the optimal thresholds for AccLLR accumulation, details of which are provided  
457 in the Methods section (see also Figure 6). Trial-by-trial onset and selection latency decoding  
458 performance were significantly worse than the chance level in most sessions (Figure 6b). Error  
459 rates for most LFP sessions were below the chance level (probability of target detection is  
460 achieved by random selection) for both onset and selection. For the onset latency, there are only  
461 two detection scenarios, whether the signal can be classified as category 1 (the pattern of spike/  
462 LFP response to a stimulus) or category 2 (the animal is alert but not hearing any sound).  
463 Hence, the probability of detection by chance is 0.5. For selection latency, the probability of  
464 detection by chance is 0.67 since there are three possibilities in a given datum (PT, Coo, or pre-  
465 stimulus baseline). Fig 6b unambiguously illustrates that error rates for selection latency  
466 detection from spikes and LFPs were mostly lower than chance level indicating superior  
467 performance of the AccLLR technique. Typically, recording sites with good onset detection  
468 also yielded superior selection detection and decoding from LFPs were more reliable with more  
469 consistent error rates over sessions.

470

471 **Discussion**

472 Using two measures, *onset latency* for detecting the presence of sound in the environment and  
473 *selection latency* for identifying stimulus specific neural codes in primate auditory cortical areas  
474 we aim to characterize the functional pathways of underlying information processing. We  
475 observed a trend in which LFP onset/ selection latencies were shorter than spike onset/ selection  
476 latencies by applying ms-by-ms t-test on time series data. However, the trial-averaged  
477 techniques do not allow the measure of stimulus-specific selection latencies since a distribution  
478 of “Pure tone trials” is used to identify the time of selection from a distribution of “Coo trials”.  
479 AccLLR analysis of our data refined the statistical significance of the trends and helped to  
480 mathematically define stimulus-specific selection latencies. In a trial-averaged analysis using  
481 the t-test on raw data as well as AccLLRs, a single numerical value of selection latency was  
482 obtained for all trials within a session and by construction across two stimulus categories.  
483 Hence, not surprisingly, latencies computed by AccLLR exhibited variability that were orders  
484 of magnitude smaller than trial-averaged tests. Both trial-averaged analysis and AccLLR at the  
485 level of single trials as well as accuracy matched pooled trials yielded similar values for LFP  
486 onset latencies across A1 and LB. This reinforces the view that areas A1 and LB may process  
487 simple stimuli in parallel. Except in case of A1 and PT stimulus, all three onset scenarios had  
488 LFP latencies preceding spike latency when accuracy was matched. Proximity of spike and LFP  
489 latency typically indicates a central role of the recorded brain area in neuronal processing, Thus  
490 our observations highlight area A1’s dominant role in coding pure tones, whereas coding of  
491 complex stimulus such as Coo and in areas higher order than A1 are more mixed in nature.  
492 Selection latencies for each trial category can be only obtained from AccLLR analysis. Shorter  
493 LFP selection latencies for A1 than LB suggest information arrival in auditory brain areas can  
494 occur hierarchically. Interestingly both single-trial decoding as well as performance matched

495 pooled trial analysis showed non-significant differences between LFP and Spike selection  
496 latency in LB; in particular the performance matched analysis revealed that LFP selection  
497 latencies had a trend of preceding spike selection latency thus reflecting a greater involvement  
498 of higher order LB area in neuronal stimulus discrimination.

499         There is a substantial literature on subdivisions of auditory cortical areas and their roles  
500 in processing complex sounds (Romani et al., 1982, Rauschecker et al., 1995, Eggermont, 1998,  
501 Bendor and Wang, 2008, Ghazanfar et al., 2008, Recanzone, 2008, Kuśmierk and  
502 Rauschecker, 2009, Bandyopadhyay et al., 2010, Kikuchi et al., 2010, Camalier et al., 2012,  
503 Sundberg et al., 2012, Niwa et al., 2013, Kikuchi et al., 2014). In this study, we investigated  
504 one such complex sound, viz., a Coo, that can be represented spectro-temporally as containing  
505 higher harmonics of a specific fundamental frequency (Figure 2), as opposed to a simple sound  
506 consisting of a single frequency. The animals were trained to respond to a stimulus that had no  
507 periodic temporal structure (pink noise), but that required them to allocate equivalent levels of  
508 attention to both simple and complex sounds (PTs and Coos, respectively). A traditional, trial-  
509 averaged analysis of the data indicated that the spike-onset latency for the pure tone was shorter  
510 in A1 than in LB (Kikuchi et al., 2014). However, there was a minimal difference in latency  
511 between A1 and LB for Coo sounds, a finding that may seem surprising from the perspective of  
512 serial hierarchical information processing. We argue that an effective way to tease out the entire  
513 processing architecture is to look at simultaneous measurements of inputs and output of a brain  
514 area using both spike and local field potential (LFP) recordings. We showed that stimulus-  
515 specific spike and LFP responses are present in A1 and LB, as found in previous studies  
516 (Ghazanfar et al., 2005, Ghazanfar et al., 2008). We then compared single-trial latencies from  
517 spike trains and LFPs at the same electrode and across different electrodes. This presents a

518 unique way to extract the local functional connectivity in auditory cortex underlying complex  
519 sound processing.

520 Latency comparison has been used previously to estimate functional neural circuitry  
521 underlying complex tasks (DiCarlo and Maunsell, 2005, Hung et al., 2005, Buschman and  
522 Miller, 2007, Monosov et al., 2008). The key methodological innovation in the current paper is  
523 employing the AccLLR framework, which allows single-trial decoding of latencies from  
524 spike/LFP data (Figure 5). Using AccLLR, we were able to evaluate latencies statistically  
525 within one session as well as compare them across sessions and thereby enhance the statistical  
526 power of our results. A somewhat similar approach based on the computation of a "surprise  
527 index" was proposed earlier by Hanes and colleagues (Hanes et al., 1995). For comparison, we  
528 also performed the latency analysis by applying the commonly used method employing a ms-  
529 by-ms rank sum test (Figure 4). Comparison of Figure 4 and Figure 5 (AccLLR results)  
530 illustrate a dramatic improvement in statistical significance of results for the trial-by-trial  
531 analysis. The trial-by-trial analyses as well as pooled trial analysis (accuracy matched) confirm  
532 the pattern of results reported by Kikuchi et al. (2014): spike onset latencies were shorter in A1  
533 than in LB for pure tones but close to each other for Coos. Error rates from decoded LFPs were  
534 higher than corresponding spike-analysis sessions, though across sessions decoding was better  
535 than chance, indicating the robustness of the information contained in LFPs. Robust decoding  
536 using LFPs was also reported in earlier studies (Hung et al., 2005, Markowitz et al., 2011,  
537 Bansal et al., 2012).

538

539 ***Functional neural circuitry underlying auditory processing***

540 A central aim of the current study was to compare latencies of spike and LFP responses in two  
541 different contexts – at onset and during neuronal selection. Latencies were compared across  
542 stimuli (PT vs. Coo) to investigate the stimulus-specific components. A key result from  
543 AccLLR analyses (both trial-by-trial and performance matched) was the nearly identical LFP  
544 onset latency in A1 for PTs and Coos and the very similar onset latencies in LB for these two  
545 stimulus categories (Figures 4 and 5). If we consider LFPs to be coupled more to inputs, the  
546 information related to the presence of an auditory stimulus in the environment arrives at both  
547 brain areas simultaneously. Previous studies demonstrated that A1 and LB receive inputs in  
548 parallel from subcortical structures, which may be the reason that there is little difference in  
549 LFP onset latencies across the two areas (Rauschecker et al., 1997, de la Mothe et al., 2006). In  
550 the case of sensory areas, where feed-forward connections dominate, relative spike latency can  
551 indicate a putative area’s contribution to information processing (VanRullen et al., 2005). In our  
552 findings, spike onset latency was usually longer than LFP onset latency in agreement with  
553 previous studies in sensory areas (Eggermont, 1998, Sundberg et al., 2012). We observed that  
554 the spike onset latency computed from trial-averaged data is shorter in A1 than in LB for pure  
555 tones but not for Coos. The also followed this trend. Interestingly, spike onset latency for Coo  
556 in LB was shorter than spike onset latency for PT using both single trial and performance  
557 matched AccLLR analyses (though a clear trend was observed in the latter analysis that  
558 matched trial-by-trial results, the latency differences were not significantly different). This  
559 validates the view that the auditory cortex is organized into lower-order sensory areas (e.g., A1),  
560 relevant for coding simple features such as fundamental frequencies, and (relatively) higher-  
561 order LB areas for coding more complex auditory features (Rauschecker et al., 1995, Kikuchi et

562 al., 2010). On the other hand, spike onset latencies for Coo in A1 and LB were not  
563 significantly different. This suggests that complex signals require more distributed resources for  
564 processing. The aforementioned findings were replicated when statistical analysis was applied  
565 to the data from each monkey individually (Figure 5).

566 An important point to note here is that the single-trial latencies detected by AccLLR  
567 analysis are typically longer than trial-averaged latencies or ones obtained from pooling all trials  
568 and setting detection accuracy to 100%. In an earlier stimulus onset latency detection study,  
569 Banerjee and colleagues (Banerjee et al., 2010) showed that latencies computed from trial-  
570 averaged AccLLRs can decrease by 15 ms at the expense of an increase in false-alarm rates. In  
571 our study, only the LFP onset latencies were very close among trial-averaged, pooled trial  
572 AccLLR and single trial AccLLR results. For spike onset latencies, the differences were  
573 maximal between trial-averaged and AccLLR measures and same pattern was followed in  
574 latency distributions from pooled trials. This indicates that LFPs may have the least variability  
575 in recording the presence of an auditory stimulus, and such tight time-locking is most likely due  
576 to the sub-cortical nature of the stimulus processing before it arrives in primary auditory cortex.

577 Area-specific properties in processing differences between stimuli can be investigated  
578 using selection latencies. Shorter LFP selection latencies in A1 compared to LB may reflect the  
579 hierarchical organization of these areas vis-à-vis stimulus-specific processing, e. g., dissociating  
580 simple (PT) from complex (Coo) (Figure 5). For both trial-averaged and trial-by-trial analysis,  
581 spike selection latency in LB was shorter than spike selection latencies in A1, indicating a  
582 stronger role of LB in processing stimulus-specific features. Combining this finding with the  
583 results from the onset latency analysis, we can dissociate the function of the two brain areas in  
584 computing different components of information processing in an environmental signal, i.e. just

585 the presence of sound vs the detailed features of that sound. We did not observe a stimulus-  
586 specific difference, PT compared to Coo, in LFP selection latency in the two areas ( $p = 0.57$  in  
587 A1,  $p = 0.01$  in LB, latencies reported in Table 1). The effect was robust when the analysis was  
588 performed in individual monkeys as well as when latencies were computed by pooling all trials  
589 and applying the AccLLR framework (Figure 5), though it was not present in the trial-averaged  
590 analysis from raw time series (Figure 4). We thus conclude that at least some stimulus-specific  
591 information arrives serially in these two brain areas, contrary to what we observed for LFP  
592 onset latency. An alternative possibility is that the lower-order auditory area A1 receives  
593 feedback projections from LB or other higher-order areas. Spike selection latency in A1 was  
594 longer than the LFP selection latency when both trial-averaged and trial-by-trial analyses were  
595 performed on individual monkey data as well as on the population data. When detection  
596 threshold was set at 100% in pooled trials this difference in spike-LFP selection latencies in A1  
597 was not observed.

598 On the other hand, spike selection latency in LB was comparable to the LFP selection  
599 latency, although there is a slight variability in this result when one examines the data on  
600 individual monkeys (Figure 5). Monkey1 exhibited the general trend of spike selection latency  
601 being longer than LFP selection latency, just as in the case of onset latencies. However,  
602 Monkey2 showed slightly shorter spike selection latencies than LFP selection latencies in LB  
603 (Figure 5). Earlier research has established that A1 and LB have strong reciprocal connections  
604 (de la Mothe et al., 2006, Hackett, 2011). Together, these data raise the possibility that LB has a  
605 top-down preparatory role for selection-related processing, whereas A1 is primarily involved in  
606 bottom-up gating of sensory signals.

607

608 ***Future directions & Limitations***

609 Our study provides a design-analysis framework to support neurophysiological findings that  
610 could help address questions related to functional networks at both local area-specific scales and  
611 global inter-areal scales. Such studies would shed light on task-specific network mechanisms  
612 underlying complex behavior. One limitation of the current study is that it ignores the  
613 information about the endogenous neural states present in ongoing oscillations and how such  
614 processes affect extrinsic stimulus driven processing. A recent study has shown that neuronal  
615 areas separated across large distances whose activities are coherent may also exhibit lower  
616 latencies in information processing using AccLLR (Wong et al. 2016). The same framework  
617 could also be adapted to detect the timing of oscillatory-response onsets and phase differences  
618 from the electrical activity of nearby and distant populations. Finally, AccLLR can be applied to  
619 macroscopic neural recordings such as electroencephalograms (EEG), intra-cranial EEG, and  
620 magnetoencephalograms (MEG) to estimate network mechanisms and thereby inform a wider  
621 research community.

622

623 **References**

- 624 Ahveninen J, Huang S, Nummenmaa A, Belliveau JW, Hung AY, Jaaskelainen IP, Rauschecker JP, Rossi S,  
625 Tiitinen H, Raij T (2013) Evidence for distinct human auditory cortex regions for sound location  
626 versus identity processing. *Nature communications* 4:2585.
- 627 Ahveninen J, Jaaskelainen IP, Raij T, Bonmassar G, Devore S, Hamalainen M, Levanen S, Lin FH, Sams M,  
628 Shinn-Cunningham BG, Witzel T, Belliveau JW (2006) Task-modulated "what" and "where"  
629 pathways in human auditory cortex. *Proc Natl Acad Sci U S A* 103:14608-14613.
- 630 Bandyopadhyay S, Shamma SA, Kanold PO (2010) Dichotomy of functional organization in the mouse  
631 auditory cortex. *Nat Neurosci* 13:361-368.
- 632 Banerjee A, Dean HL, Pesaran B (2010) A likelihood method for computing selection times in spiking  
633 and local field potential activity. *J Neurophysiol* 104:3705-3720.
- 634 Banerjee A, Dean HL, Pesaran B (2012) Parametric models to relate spike train and LFP dynamics with  
635 neural information processing. *Front Comput Neurosci* 6:51.
- 636 Bansal AK, Truccolo W, Vargas-Irwin CE, Donoghue JP (2012) Decoding 3D reach and grasp from hybrid  
637 signals in motor and premotor cortices: spikes, multiunit activity, and local field potentials. *J*  
638 *Neurophysiol* 107:1337-1355.
- 639 Bendor D, Wang X (2008) Neural response properties of primary, rostral, and rostromedial core fields  
640 in the auditory cortex of marmoset monkeys. *J Neurophysiol* 100:888-906.
- 641 Bizley JK, Cohen YE (2013) The what, where and how of auditory-object perception. *Nat Rev Neurosci*  
642 14:693-707.
- 643 Buschman TJ, Miller EK (2007) Top-down versus bottom-up control of attention in the prefrontal and  
644 posterior parietal cortices. *Science* 315:1860-1862.
- 645 Buzsaki G, Anastassiou CA, Koch C (2012) The origin of extracellular fields and currents--EEG, ECoG, LFP  
646 and spikes. *Nat Rev Neurosci* 13:407-420.
- 647 Camalier CR, D'Angelo WR, Sterbing-D'Angelo SJ, de la Mothe LA, Hackett TA (2012) Neural latencies  
648 across auditory cortex of macaque support a dorsal stream supramodal timing advantage in  
649 primates. *Proc Natl Acad Sci U S A* 109:18168-18173.
- 650 de la Mothe LA, Blumell S, Kajikawa Y, Hackett TA (2006) Thalamic connections of the auditory cortex in  
651 marmoset monkeys: core and medial belt regions. *J Comp Neurol* 496:72-96.
- 652 DiCarlo JJ, Maunsell JH (2005) Using neuronal latency to determine sensory-motor processing pathways  
653 in reaction time tasks. *J Neurophysiol* 93:2974-2986.
- 654 Eckhoff P, Holmes P, Law C, Connolly PM, Gold JI (2008) On diffusion processes with variable drift rates  
655 as models for decision making during learning. *New J Phys* 10:nihpa49499.
- 656 Eggermont JJ (1998) Azimuth coding in primary auditory cortex of the cat. II. Relative latency and  
657 interspike interval representation. *J Neurophysiol* 80:2151-2161.
- 658 Eggermont JJ, Munguia R, Pienkowski M, Shaw G (2011) Comparison of LFP-based and spike-based  
659 spectro-temporal receptive fields and cross-correlation in cat primary auditory cortex. *PLoS one*  
660 6:e20046.
- 661 Gawne TJ, Kjaer TW, Richmond BJ (1996) Latency: another potential code for feature binding in striate  
662 cortex. *J Neurophysiol* 76:1356-1360.
- 663 Ghazanfar AA, Chandrasekaran C, Logothetis NK (2008) Interactions between the superior temporal  
664 sulcus and auditory cortex mediate dynamic face/voice integration in rhesus monkeys. *J*  
665 *Neurosci* 28:4457-4469.
- 666 Ghazanfar AA, Maier JX, Hoffman KL, Logothetis NK (2005) Multisensory integration of dynamic faces  
667 and voices in rhesus monkey auditory cortex. *J Neurosci* 25:5004-5012.
- 668 Gold JI, Shadlen MN (2001) Neural computations that underlie decisions about sensory stimuli. *Trends*  
669 *Cogn Sci* 5:10-16.

- 670 Guo W, Chambers AR, Darrow KN, Hancock KE, Shinn-Cunningham BG, Polley DB (2012) Robustness of  
 671 cortical topography across fields, laminae, anesthetic states, and neurophysiological signal  
 672 types. *J Neurosci* 32:9159-9172.
- 673 Gusnard DA, Akbudak E, Shulman GL, Raichle ME (2001) Medial prefrontal cortex and self-referential  
 674 mental activity: relation to a default mode of brain function. *Proc Natl Acad Sci U S A* 98:4259-  
 675 4264.
- 676 Hackett TA (2011) Information flow in the auditory cortical network. *Hearing research* 271:133-146.
- 677 Hanes DP, Thompson KG, Schall JD (1995) Relationship of presaccadic activity in frontal eye field and  
 678 supplementary eye field to saccade initiation in macaque: Poisson spike train analysis. *Exp*  
 679 *Brain Res* 103:85-96.
- 680 Hind JE (1953) An electrophysiological determination of tonotopic organization in auditory cortex of  
 681 cat. *J Neurophysiol* 16:475-489.
- 682 Hung CP, Kreiman G, Poggio T, DiCarlo JJ (2005) Fast readout of object identity from macaque inferior  
 683 temporal cortex. *Science* 310:863-866.
- 684 Kayser C, Petkov CI, Logothetis NK (2007) Tuning to sound frequency in auditory field potentials. *J*  
 685 *Neurophysiol* 98:1806-1809.
- 686 Kikuchi Y, Horwitz B, Mishkin M (2010) Hierarchical auditory processing directed rostrally along the  
 687 monkey's supratemporal plane. *J Neurosci* 30:13021-13030.
- 688 Kikuchi Y, Horwitz B, Mishkin M, Rauschecker JP (2014) Processing of harmonics in the lateral belt of  
 689 macaque auditory cortex. *Frontiers in Neuroscience* 8: 204
- 690 Kreiman G, Hung CP, Kraskov A, Quiroga RQ, Poggio T, DiCarlo JJ (2006) Object selectivity of local field  
 691 potentials and spikes in the macaque inferior temporal cortex. *Neuron* 49:433-445.
- 692 Kruger J, Becker JD (1991) Recognizing the visual stimulus from neuronal discharges. *Trends in*  
 693 *neurosciences* 14:282-286.
- 694 Kuśmierk P, Rauschecker JP (2009) Functional specialization of medial auditory belt cortex in the alert  
 695 rhesus monkey. *J Neurophysiol* 102:1606-1622.
- 696 Kuśmierk P, Rauschecker JP (2014) Selectivity for space and time in early areas of the auditory dorsal  
 697 stream in the rhesus monkey. *J Neurophysiol* 111:1671-1685.
- 698 Markowitz DA, Wong YT, Gray CM, Pesaran B (2011) Optimizing the decoding of movement goals from  
 699 local field potentials in macaque cortex. *J Neurosci* 31:18412-18422.
- 700 Merzenich MM, Kaas JH, Roth GL (1976) Auditory cortex in the grey squirrel: tonotopic organization  
 701 and architectonic fields. *J Comp Neurol* 166:387-401.
- 702 Middlebrooks JC, Clock AE, Xu L, Green DM (1994) A panoramic code for sound location by cortical  
 703 neurons. *Science* 264:842-844.
- 704 Monosov IE, Trageser JC, Thompson KG (2008) Measurements of simultaneously recorded spiking  
 705 activity and local field potentials suggest that spatial selection emerges in the frontal eye field.  
 706 *Neuron* 57:614-625.
- 707 Morel A, Garraghty PE, Kaas JH (1993) Tonotopic organization, architectonic fields, and connections of  
 708 auditory cortex in macaque monkeys. *J Comp Neurol* 335:437-459.
- 709 Muscari C, Turinetti B, Coli G, Galeazzi M, Cattabriga I, Finelli C, Biagetti L, Guarnieri C, Caldarera CM  
 710 (1990) Changes in myocardial mitochondrial respiration after ligation of the coronary artery in  
 711 pigs. *Cardioscience* 1:261-264.
- 712 Nawrot MP, Aersten A, Rotter S (2003) Elimination of response latency variability in neuronal spike  
 713 trains. *Biol Cybern* 88:321-334.
- 714 Nielsen KJ, Logothetis NK, Rainer G (2006) Dissociation between local field potentials and spiking  
 715 activity in macaque inferior temporal cortex reveals diagnosticity-based encoding of complex  
 716 objects. *J Neurosci* 26:9639-9645.

- 717 Niwa M, Johnson JS, O'Connor KN, Sutter ML (2013) Differences between primary auditory cortex and  
718 auditory belt related to encoding and choice for AM sounds. *J Neurosci* 33:8378-8395.
- 719 Rauschecker JP, Tian B, Hauser M (1995) Processing of complex sounds in the macaque nonprimary  
720 auditory cortex. *Science* 268:111-114.
- 721 Rauschecker JP, Tian B, Pons T, Mishkin M (1997) Serial and parallel processing in rhesus monkey  
722 auditory cortex. *J Comp Neurol* 382:89-103.
- 723 Recanzone GH (2008) Representation of con-specific vocalizations in the core and belt areas of the  
724 auditory cortex in the alert macaque monkey. *J Neurosci* 28:13184-13193.
- 725 Romani GL, Williamson SJ, Kaufman L (1982) Tonotopic organization of the human auditory cortex.  
726 *Science* 216:1339-1340.
- 727 Scott BH, Malone BJ, Semple MN (2011) Transformation of temporal processing across auditory cortex  
728 of awake macaques. *J Neurophysiol* 105:712-730.
- 729 Sheline YI, Raichle ME, Snyder AZ, Morris JC, Head D, Wang S, Mintun MA (2010) Amyloid plaques  
730 disrupt resting state default mode network connectivity in cognitively normal elderly. *Biological*  
731 *psychiatry* 67:584-587.
- 732 Sundberg KA, Mitchell JF, Gawne TJ, Reynolds JH (2012) Attention influences single unit and local field  
733 potential response latencies in visual cortical area V4. *J Neurosci* 32:16040-16050.
- 734 Thompson KG, Hanes DP, Bichot NP, Schall JD (1996) Perceptual and motor processing stages identified  
735 in the activity of macaque frontal eye field neurons during visual search. *J Neurophysiol*  
736 76:4040-4055.
- 737 Tian B, Kuśmierk P, Rauschecker JP (2013) Analogues of simple and complex cells in rhesus monkey  
738 auditory cortex. *Proc Natl Acad Sci U S A* 110:7892-7897.
- 739 Tian B, Rauschecker JP (2004) Processing of frequency-modulated sounds in the lateral auditory belt  
740 cortex of the rhesus monkey. *J Neurophysiol* 92:2993-3013.
- 741 Van Rullen R, Thorpe SJ (2001) Rate coding versus temporal order coding: what the retinal ganglion  
742 cells tell the visual cortex. *Neural Comput* 13:1255-1283.
- 743 VanRullen R, Guyonneau R, Thorpe SJ (2005) Spike times make sense. *Trends in neurosciences* 28:1-4.
- 744 Wald A, Wolfowitz J (1947) Optimum character of the sequential probability ratio test. *AnnMath Statist*  
745 19:326-329.
- 746 Wong YT, Fabiszak MM, Novikov Y, Daw ND, Pesaran B.(2016) Coherent neuronal ensembles are rapidly  
747 recruited when making a look-reach decision. *Nature Neuroscience*, 19(2), 327-34.
- 748
- 749
- 750

751 TABLE 1: Mean neuronal latencies for onset and selection of auditory stimulus with standard  
 752 error of the mean (SEM) reported in parentheses. The sample sizes are indicated at the  
 753 beginning of each column in parentheses and underlined. The numbers for A1 are presented in  
 754 bold and LB in italics for ease of view.

Signal	Area	Onset (ms)		Selection (ms)		
		PT ( <u>56</u> )	Coo ( <u>56</u> )	PT-Coo ( <u>56</u> )		
LFP	A1	<b>45(4.0)</b>	<b>29 (1.93)</b>	<b>111 (16.86)</b>		Trial averaged (t-test on raw data)
	<i>LB</i>	<i>58 (6.76)</i>	<i>45(5.65)</i>	<i>121 (13.77)</i>		
Spike	A1	<b>87(10.36)</b>	<b>63 (5.47)</b>	<b>140 (15.55)</b>		
	<i>LB</i>	<i>103(13.11)</i>	<i>83 (8.86)</i>	<i>164 (26.15)</i>		
		PT ( <u>56</u> )	Coo ( <u>56</u> )	PT-Coo ( <u>56</u> )		Trial averaged (t-test on AccLLR)
LFP	A1	<b>60 (7.13)</b>	<b>51 (5.8)</b>	<b>155 (22.57)</b>		
	<i>LB</i>	<i>57 (5.59)</i>	<i>55 (7.37)</i>	<i>170 (22.19)</i>		
Spike	A1	<b>67 (10.54)</b>	<b>74 (6.15)</b>	<b>89 (16.54)</b>		
	<i>LB</i>	<i>87(11.76)</i>	<i>94 (11.43)</i>	<i>106 (20.91)</i>		
		PT ( <u>15319</u> )	Coo ( <u>15326</u> )	PT ( <u>13825</u> )	Coo ( <u>14035</u> )	AccLLR: Trial-by-trial
LFP	A1	<b>35 (0.22)</b>	<b>31 (0.21)</b>	<b>113 (1.04)</b>	<b>111 (1.03)</b>	
	<i>LB</i>	<i>36 (0.32)</i>	<i>39 (0.29)</i>	<i>161 (1.38)</i>	<i>167 (1.48)</i>	
Spike	A1	<b>52 (0.40)</b>	<b>69 (0.46)</b>	<b>187 (1.64)</b>	<b>178 (1.77)</b>	
	<i>LB</i>	<i>92 (0.56)</i>	<i>66 (0.33)</i>	<i>163 (1.67)</i>	<i>155 (1.77)</i>	
<u>LFP</u>	A1	<b>38 (3.4)</b>	<b>26 (2.7)</b>	<b>62 (3.1)</b>	<b>58 (2.32)</b>	AccLLR: 100% accuracy matched pooled trials
	<i>LB</i>	<i>30 (3.06)</i>	<i>31 (2.9)</i>	<i>90 (8.0)</i>	<i>84 (7.15)</i>	
<u>Spike</u>	A1	<b>39 (3.4)</b>	<b>48 (4.45)</b>	<b>69 (5.48)</b>	<b>75 (7.5)</b>	
	<i>LB</i>	<i>49 (5.3)</i>	<i>41 (4.3)</i>	<i>83 (8.02)</i>	<i>78 (7.33)</i>	

755

756

757 **Figure Captions**

758 FIGURE 1: a) Simultaneous recordings from two arbitrary brain areas 1 and 2. On the right, we  
759 illustrate the definition of onset latencies (OL) and selection latencies (SL) by plotting the spike  
760 response (left panel) and local field potential (LFP; right panel) from each recording site. Onset  
761 latency is computed using an event as model 1 in the AccLLR framework (Banerjee et al.,  
762 2010) and pre-stimulus baseline as model 2 (see equation 1 in Methods section). Selection  
763 latency is computed using pure-tone stimulus as model 1 and Coo as model 2; b) the effective  
764 network architectures inferred from different onset latency values. The solid lines reflect the  
765 effective network connections, whereas the dotted lines indicate a less likely connection that can  
766 be inferred from latency measures.

767

768 FIGURE 2: Experimental design, Go/No-go task. a) Monkey waits during a rest period with  
769 hands on a lever and attends to the stimuli (pure tone, Coo, or pink noise; presentation time, 300  
770 ms). To obtain a water reward, the monkey must release the lever when pink noise is presented.  
771 The next trial starts 600 ms after the previous stimulus onset. b) The spectrogram (time,  
772 frequency, and power) of pure-tone and Coo stimuli. The frequency of pure tones matches the  
773 fundamental frequency of the Coo.

774

775 FIGURE 3: One representative session from each monkey, where simultaneous recordings from  
776 two areas spikes and LFP could be obtained. First row indicates spike rasters (cyan and magenta  
777 dots) and firing rates (blue and red) computed using Gaussian smoothing (10 ms window) for  
778 pure-tone (PT: cyan/blue) and Coo (magenta/red) stimuli. The second row depicts the trial-by-  
779 trial LFP waveforms using the same color code as for spikes. The averaged LFP responses are

780 plotted in blue and red. The spike-LFP responses in two auditory cortical areas A1 and LB were  
781 recorded during the same session in each monkey.

782

783 FIGURE 4: a) Estimation of *trial-averaged* onset and selection latency using ms-by-ms t-test on  
784 raw time series. For spikes, the binary time series was transformed to a spike density function  
785 (SDF) by convolving single trial spike trains with assymetric exponential functions having  
786 different growth and decay time constants, 1 ms and 20 ms respectively following Thompson et  
787 al (1996). A ms-by-ms t- test was performed on the distribution SDF's in a given session from  
788 different conditions (see text for details). For onset, pre-stimulus rest period was used to  
789 compute the spike density function (SDF). Analyses were performed across both monkeys and  
790 for each monkey individually. Error bars were plotted at 95% significance levels.

791 b) Estimation of trial-averaged onset and selection latency from AccLLR distributions using ms  
792 by ms t-test.  $p=0.01$  was chosen as threshold for significance.

793

794 FIGURE 5: a) Estimation of *trial-by-trial* onset and selection latency using AccLLR. We follow  
795 the same pattern of presentation as in Figure 4 and report the group-level analysis and individual  
796 monkey analysis. Error bars were computed at 95% significance levels by pooling all trials and  
797 sessions in a monkey. See text for details of Methods. b) Estimation of *trial-by-trial* onset and  
798 selection latency using AccLLR on pooling all trial information within a stimulus category to a  
799 single trial in each session and setting accuracy to 100%. Error bars were computed at 95%  
800 significance levels.

801

802 FIGURE 6: Decoding performance using AccLLR. a) Setting up the bounds of accumulation is  
803 an integral part of AccLLR analysis. The probability of correct detection varies with where the  
804 bound is set for both spikes and LFPs. Furthermore, the onset latency also varies with the  
805 selection of thresholds and, consequently, with the probability of correct detection. Optimal  
806 onset latency detection is defined when the threshold for the false positive rate for pre-stimulus  
807 data (null) equals or exceeds the detection of true positives from event (post-stimulus period)  
808 data. For selection latency, there are three possibilities: PT, Coo, or "don't know" (baseline).  
809 Here the optimal threshold was chosen when the probability of correct detection matched the  
810 probability of "don't knows" from the rest period (null) data. b) Error rates of decoding from  
811 spikes (1<sup>st</sup> column) and LFPs (2<sup>nd</sup> column). Error rates for Onset (1<sup>st</sup> row) and Selection latency  
812 (2<sup>nd</sup> row) are also shown in matching color codes. Note that y-axis is error, lower error indicates  
813 better performance.

814

815

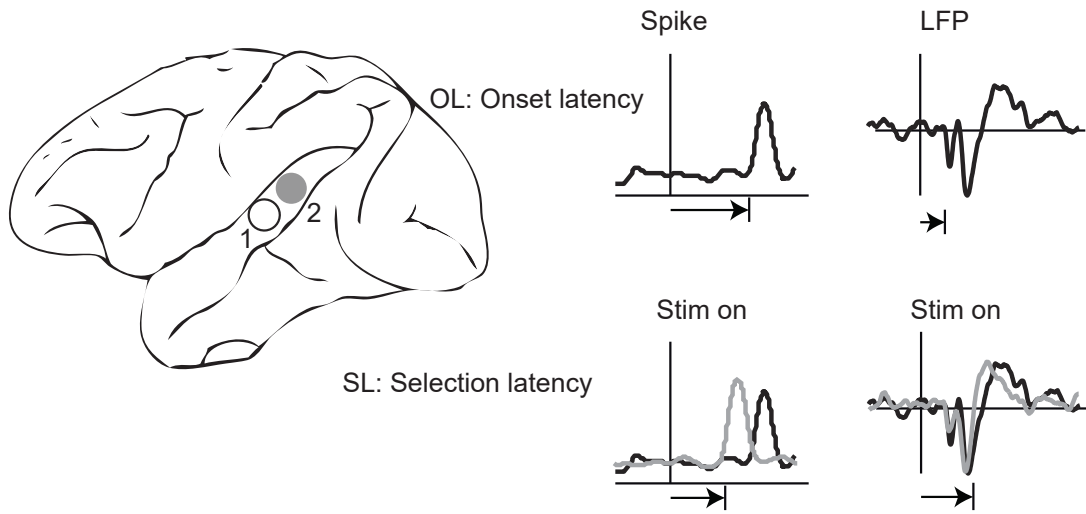
816

817

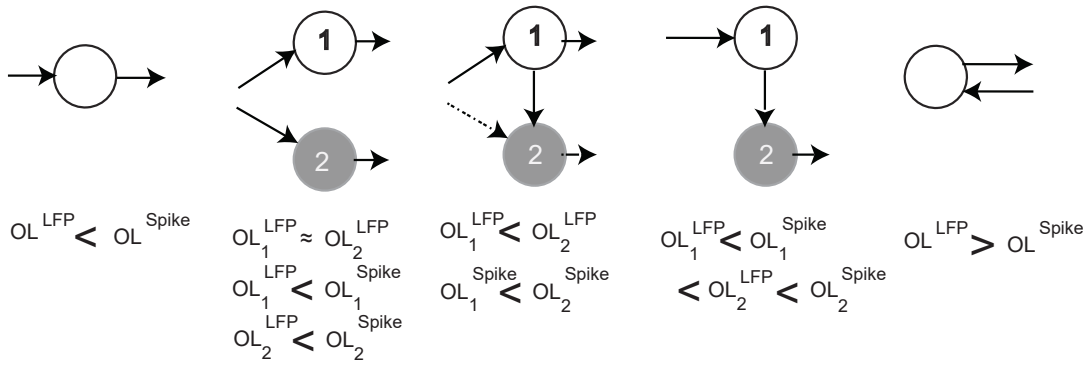
818

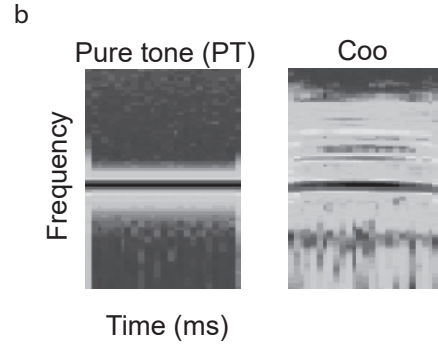
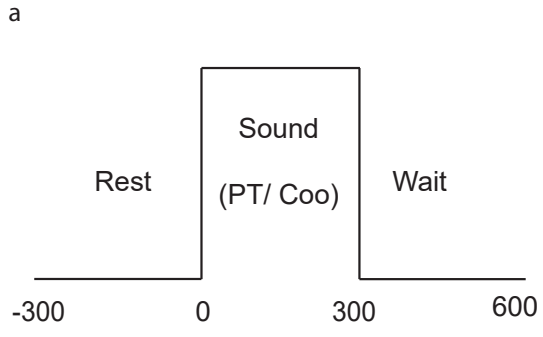
819

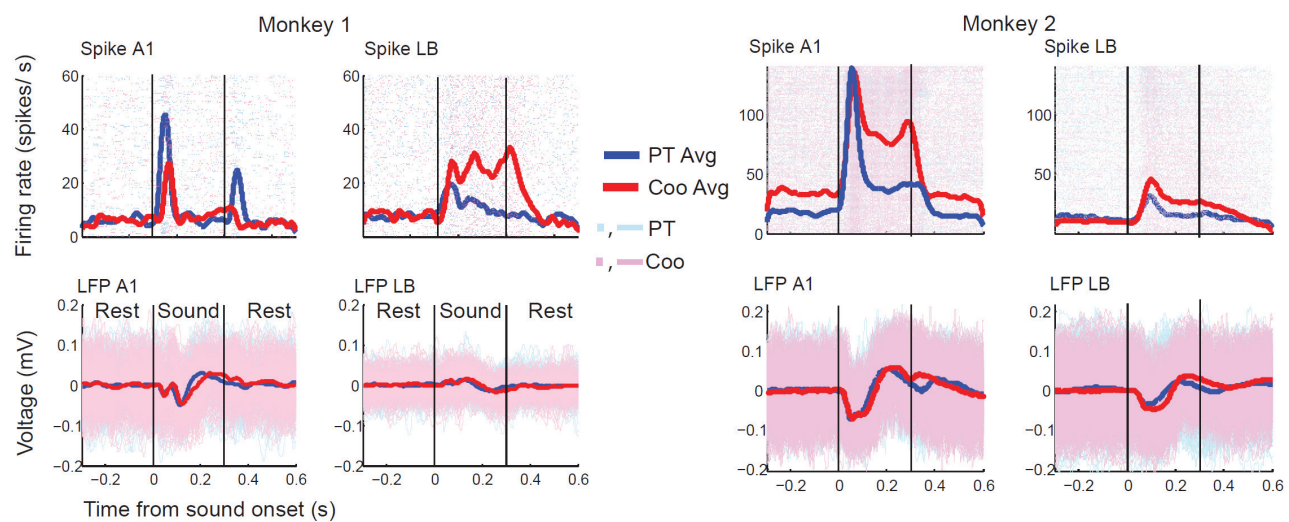
a



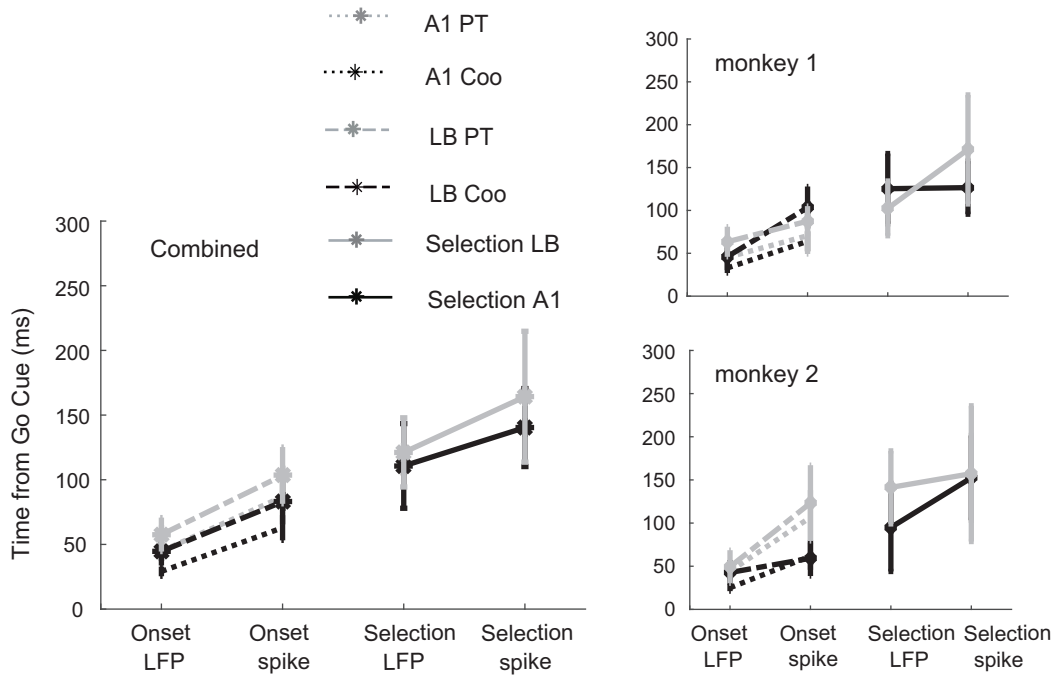
b



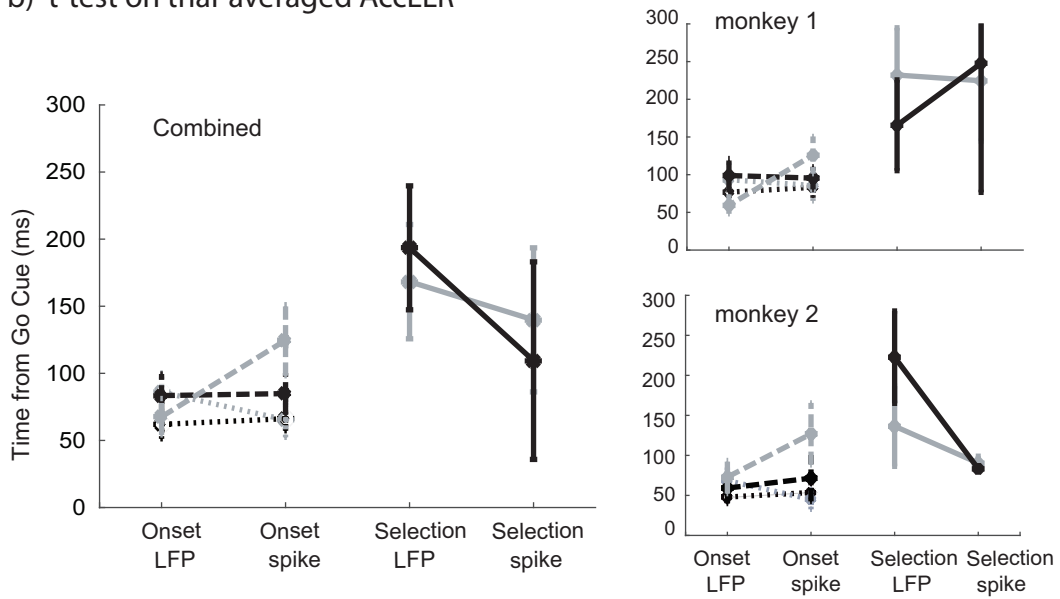




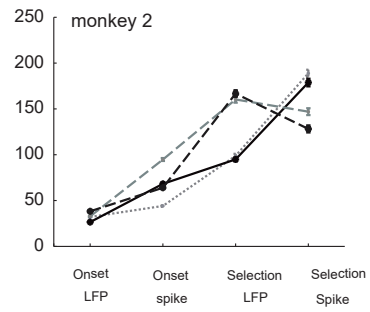
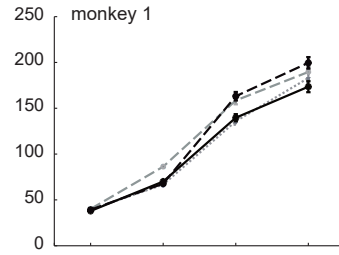
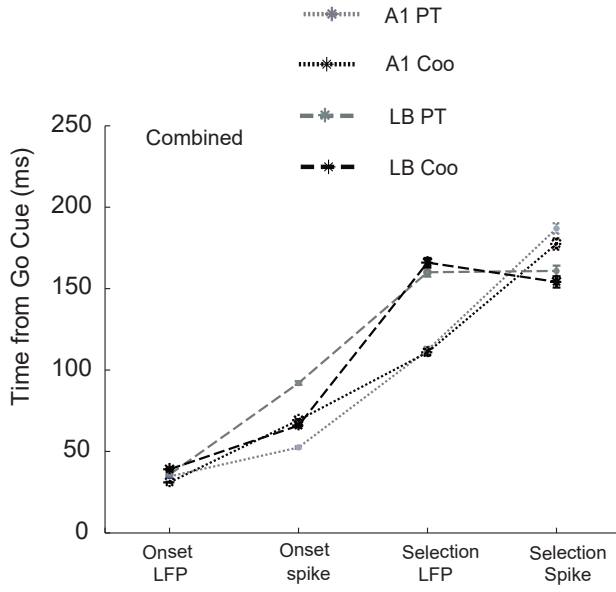
a) t-test on raw data



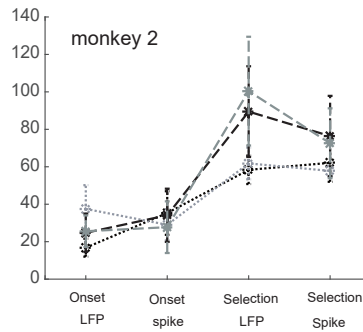
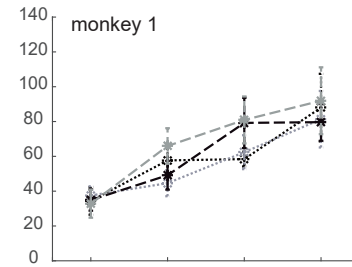
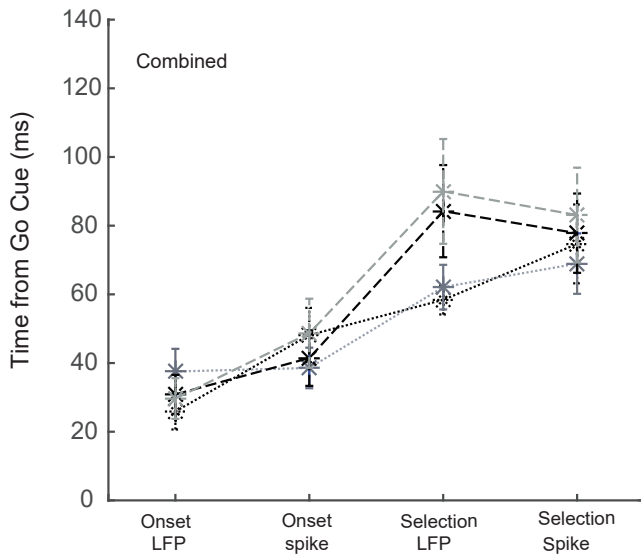
b) t-test on trial-averaged AccLLR



a) Single trial estimates

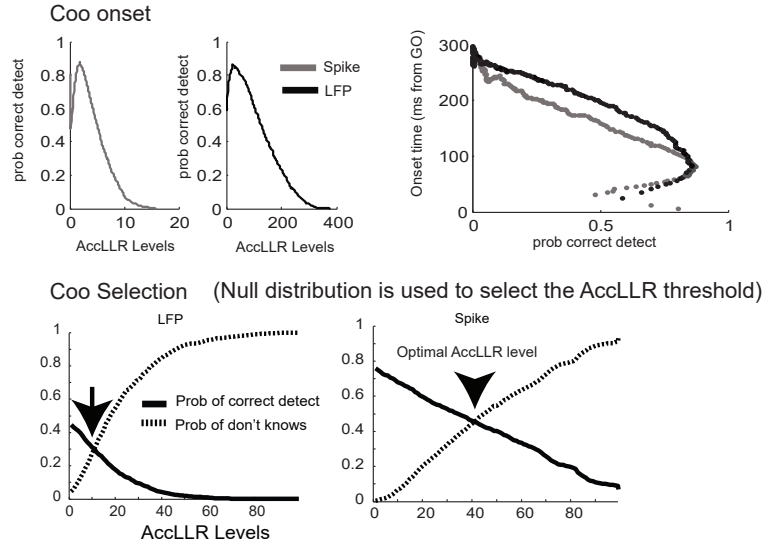


b) Pooled trial estimates with accuracy 100%



a

Optimal threshold detection for onset and selection



b

Error rates with optimal thresholds

